Systematic changes of the Nb-Sn reaction with time, temperature and alloying in Restacked-Rod-Process (RRP) Nb_3Sn strands

A. K. Ghosh, E. A. Sperry, J. D'Ambra, and L. D. Cooley

***Abstract*— Reaction heat treatments spanning 605 to 750 °C and 24 to ~400 hours were applied to several sets of RRP strands. Magnetization and transport measurements were used to track the changes of superconducting properties and the amounts of Nb_3Sn formed. The experiments showed that temperature increases of 15 °C produced equivalent properties in half the time within the temperature range 620-680 °C. This result was the same whether Ta or Ti was used to alloy the Nb_3Sn. The bulk pinning force F_p for Ta-alloyed wires displayed a significant drop for temperatures outside the range above, due to tin gradients at low temperatures and grain growth at high temperatures. The F_p drop at high reaction temperatures prevents wire technology from taking advantage of significantly higher Kramer-plot intercept H_K for high-temperature reactions. On the other hand, Ti alloying provides a quick and potent means to increase H_K at reaction temperatures for which F_p remains high.**

***Index Terms*—Niobium-Tin compounds, electric variables measurements, magnetic susceptibility.**

I. Introduction

NIOBIUM-TIN strand technology is now mature, with performance, reproducibility, lot size, and cabling robustness fulfilling engineering needs for high field magnets, such as large aperture >200 $T \cdot m^{-1}$ quadrupoles for the LHC Accelerator Research Program (LARP) [1]. The present state of Nb_3Sn wire art routinely achieves critical current density J_c well above 3000 $A \cdot mm^{-2}$ in the non-copper region at 12 T and 4.2 K, with champion values >3,200 $A \cdot mm^{-2}$ at 12 T as well as >1,650 $A.mm^{-2}$ at 15 T.

In this paper, we explore more widely the limits to strand technology, specifically in Restack-Rod-Process (RRP®) strands manufactured by Oxford Instruments – Superconducting Technology (OST). This strand design has several key characteristics [2]. By restacking copper-clad niobium-alloy rods, support for tin diffusion from a large central core is provided by the resulting copper network. The diffusion network helps by allowing much of the reacted A15 region to be near 25% Sn while also increasing the region's homogeneity. This is in contrast to powder-in-tube and rod-in-tube designs, for which radial tin diffusion is bottlenecked by the formation of high-tin compounds and the lack of a bypass for radial tin composition gradients. In addition, alloying elements can be distributed in the stacked-rod annulus by choosing Nb7.5wt.%Ta (Nb7.5Ta) rods and/or distributing a number of Nb47wt.%Ti (Nb47Ti) rods in the layout. This mitigates the bottleneck caused by Nb-Sn-Cu-Ti and Nb-Ta-Sn-Cu-Ti intermetallics at the core-annulus interface [3].

Reducing tin gradients has now been recognized as a crucial need [4-7], because the weak superconducting properties of low-tin regions become averaged with the strong properties of high-tin regions, reducing the performance by a significant amount (~30% [5]). It is somewhat surprising, therefore, that the best RRP strands contain sub-elements resembling solid tubes after reaction, because the growth and merging of the Nb-alloy rods during their conversion to Nb_3Sn pinches off the diffusion network. Evidently, a thin copper network is sufficient to provide a high A15 area fraction while also mitigating gradients. Measurements by Lee and Larbalestier [6] show that the average radial gradient across the A15 annulus is only ~0.6% Sn over 20 μm in RRP strands, far less than the ~3% variation over the same distance in powder-in-tube wires, both for samples reacted to tin exhaustion at 675 °C.

In this paper we exploit the facts that RRP strands mitigate gradients, yet produce tube-like A15 layers. As in the past [4-6], tube-like layers permit examination of superconducting properties by magnetometry. We explore a wide range of temperatures and reaction times to adjust critical temperature T_c, the Kramer-plot extrapolated irreversibility field H_K, and the grain size. This provides a means to assess more fully the limits of performance, since J_c is a product of flux-pinning in the A15 region and the area fraction of A15, while the flux-pinning properties of the A15 region depend on T_c and H_K [5].

Samples from billets manufactured under the US Conductor Development Program (CDP) [8] were studied. The LARP baseline RRP-8220 is a Ta-alloyed design (about 4 at.% Ta) with Nb7.5Ta rods around a Sn alloy core. RRP-8079 is a Ti-alloyed billet where the Ti is introduced by distributing Nb plus Nb47Ti rods around a Sn core [9]. This billet has a Ti:Nb ratio of 2.4 at% in the annulus The cross-sections of the two wires at 0.7 mm diameter are shown in Fig. 1. RRP-8220 con-

Manuscript received August 29, 2008. This work supported by the U.S. Department of Energy under Contract No. DE-AC02-98CH10886.

A. K. Ghosh, E. A. Sperry and J. D'Ambra, are with the Magnet Division, Brookhaven National Laboratory, Upton, NY 11973, USA (corresponding author, phone: 631-344-3974; fax: 631-344-2190; e-mail: aghosh@bnl.gov).

L. D. Cooley was with Brookhaven National Laboratory, and is now with Fermi National Accelerator Laboratory, Batavia, IL 60510, USA (e-mail: ld-cooley@fnal.gov).

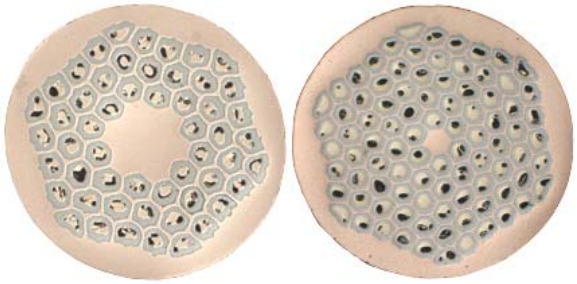

Fig. 1. Strand cross-section of RRP-8820 (left) and RRP-8079 (right).

tains 54 sub-elements with a diameter of 70 μm, whereas 8079 contains 90 sub-elements with a diameter of 57 μm. Because RRP-8079 and RRP-8220 are not design analogs, we also examine Ti-alloyed RRP-9415 (2.0 at% Ti in the annulus) and Ti+Ta alloyed RRP-9362 (0.6 at.% Ti + 4 at.%Ta), both of which are 54-subelement analogs of RRP-8220.

II. MEASUREMENTS AND PROCEDURES

Strand samples were reacted in vacuum on stainless steel barrels and then transferred to Ti-6Al-4V alloy test barrels. All wires were reacted at 210 °C and 400 °C, for 48 h at each stage. The final A15 formation reaction times and temperatures were varied between 605 and 750 °C and 48 to 384 h. As nomenclature, we indicate e.g. 605/48 to represent a final reaction at 605 °C for 48 hours.

The critical current, I_c, at 4.2 K was measured at BNL as a function of field as described earlier [10]. Voltage-current (V-I) data were acquired in 0.5 T intervals from 8 T to the 11.5 T limit of our magnet to determine J_c (criterion: 10^{-14} Ω-m). The product $J_c^{0.5}H^{0.25}$ plotted vs. field H (a Kramer plot) could be fit by a line with a high degree of accuracy, and this fit was used to determine J_c at the 12 T conductor benchmark field, the zero-current intercept H_K, and the maximum bulk pinning force $F_{p,\,max} = J_c(0.2H_K) \cdot 0.2\ \mu_0 H_K$. Note that J_c(12 T) is quoted without self-field correction, whereas for H_K and $F_{p,\,max}$ a self-field correction was applied to the $J_c(H)$ data prior to fitting. The self-field due to the transport current for 0.7 mm diameter wire is 0.57 mT·A^{-1}.

Since the Nb_3Sn region is an annular ring surrounding the large Cu-Sn core and bounded by the Nb barrier after reaction, we repeat the magnetic analyses used in past work [3],[5] to determine superconducting properties. The decrease of tin content with increasing radius has been verified by microchemistry analysis on RRP wires [7], validating the requirement that shielding-current loops do not mask the electromagnetic behavior inside them. The magnetic moment of 5-7 mm long samples was measured with the field co-axial to the strand using a commercial SQUID magnetometer. The samples were cooled to 5 K in zero field and then warmed to 20 K in 10 mT field. Magnetic moment data was then normalized to the moment at 5 K. The transition at 9.2 K is due to the Nb diffusion barrier, which is initially about 17% of the area of the sub-element and was partially reacted for some samples.

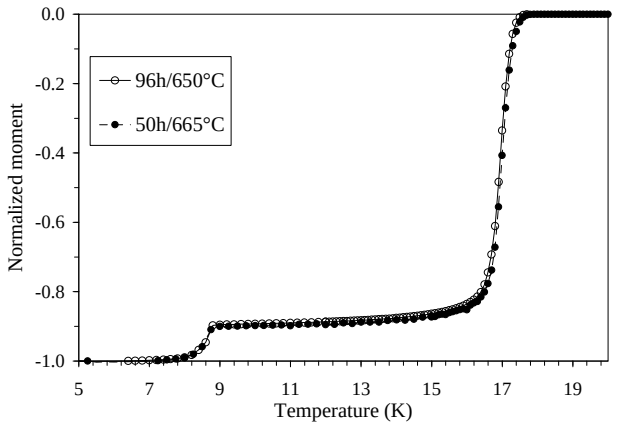

Fig. 2. Magnetic moment curves for two samples of RRP 8220. Nearly identical magnetic moment curves are observed for samples reacted at 650 °C for 96 hrs and 665 °C for 48hrs.

T_c is defined as the mid-point of the transition above 9.2 K and the width ΔT_c is defined as being between 10% and 90 % of the magnetometer signal at 9.2 K. T_c can be mapped to the average Sn composition in the A15 phase assuming the linear dependence found by Devantay *et al.* [11]:

$$T_C = 6 + 12\left[(\%Sn - 18)/7\right]. \quad (1)$$

III. RESULTS AND DISCUSSION

A. Baseline: Ta-alloyed RRP-8820

Table I summarizes the reaction parameters and the properties for RRP-8220 samples. There are several observations to make from these data. First, temperature increases of 15 °C produce equivalent behavior in approximately half the final reaction time. The equivalency can be quite remarkable—as seen in Fig. 2, the 650/96 and 665/50 reactions gave almost identical moment vs. temperature data. By implication, the geometry and composition of the A15 regions must also be nearly identical, and so too the other properties for 650/96 and 665/50 listed in Table I. Further inspection of Table I shows

TABLE I. SUMMARY OF REACTION PARAMETERS AND MEASUREMENTS FOR RRP 8220 STRANDS

Temp °C	Time h	J_c(12T) A/mm^2	RRR	H_K T	T_c K	ΔT_c	$F_{p,max}$ GN/m^3
605	150	2437	411	22.0	16.34	1.10	58.1
620	96	2722	450	22.5	16.53	1.20	62.6
620	192	2892	377	22.9	16.64	1.35	64.8
620	384	2909	74	23.8			61.3
635	48	2571	364	22.4	16.53	1.25	61.2
650	48	2890	305	23.1	16.77	1.03	65.2
650	96	3072	233	23.5	16.92	0.85	67.3
665	50	2987	171	23.8	16.92	0.85	64.3
680	48	3060	109	25.1	17.10	1.13	61.0
695	48	3114	56	26.4	17.32	1.00	57.2
750	96	2371	15	27.3	17.24	1.35	40.6

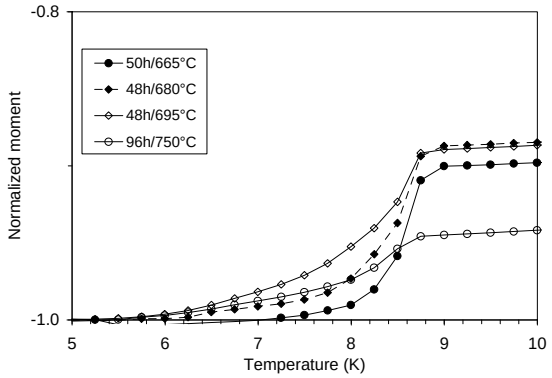

Fig. 3. Magnetic moment curves for RRP-8220 reacted at the higher temperatures, showing the changes at the 9.2 K transition and the development of a tail below 9.2 K

that this relationship is obeyed generally between 620 and 665 °C, e.g. between 620/96 and 635/48, and between 620/192 and 650/48 (two 15 °C increments). Thus, there are multiple time-temperature pathways to equivalent properties.

Second, T_c and H_K both increase systematically with increasing reaction temperature or time, implying that there is a general increase in the overall tin content as the reaction is driven more intensely. While this might seem obvious, it is curious that ΔT_c does not change appreciably, which we speculate is attributable to the rapid tin diffusion along the copper network. According to (1), the ~1.0 K ΔT_c values are consistent with the 0.6% Sn variation across the A15 region reported in [7]. The T_c values might then reflect the composition at the interface between rods (e.g. 24.6% Sn for 665/50) at the time when they merge, because at this point completion of shielding-current paths as well as blockage of the network both occur.

Third, at the highest temperature of 750 °C, T_c reduces and ΔT_c increases compared with the 695/48 data. This is in contrast to other studies [4, 6], where long hot reactions produced the highest T_c and narrowest transitions. At this stage, the Sn source is exhausted, so these data suggest that the Sn-rich A15 regions are depleted to feed the Sn-poor regions. Most of the Sn-poor regions are at the Nb diffusion barrier, as suggested by the reduction of the signal at 9.2 K, the tail below the 9.2 K transition (both shown in Fig. 3), and the drop in the copper stabilizer residual resistivity ratio *RRR*. H_K attains the highest value for RRP-8220, consistent with previous work.

In a previous paper [12] we showed that J_c reaches a broad plateau between 650 and 695 °C, and that H_K increases almost linearly with reaction temperature. Here, we point to another interesting feature of the data, the variation of J_c and $F_{p,max}$ as a function of H_K, shown in Fig. 4. While J_c has a broad plateau for H_K > 23.5 T, $F_{p,max}$ reaches a peak and reduces sharply for H_K > 23.5 T. This implies that for temperatures exceeding 650 °C, the density of grain-pinning sites is decreasing faster than can be compensated by the increase of the specific grain-boundary pinning force [7]. So, while higher temperatures favor better superconducting properties as evidenced by the higher T_c and H_K, it is not possible to take advantage of them without somehow preventing grain growth.

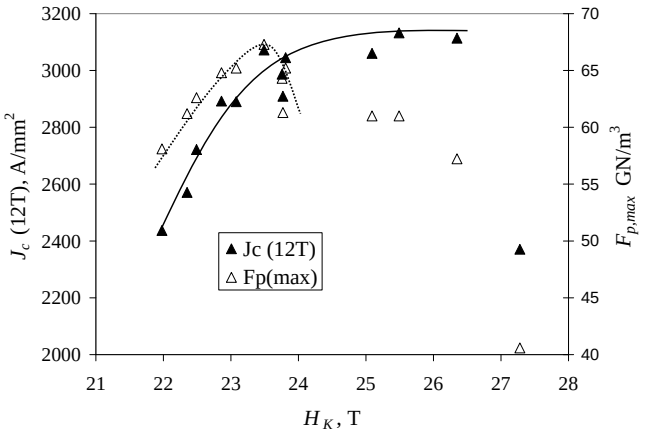

Fig. 4. Plot of J_c (12 T) and $F_{p,max}$ versus H_K for samples from RRP-8220.

B. Variations from the baseline: Ti-alloyed RRP-8709 and RRP-9415, and Ti+Ta-alloyed RRP-9362

RRP-8079 was designed with less Nb and Sn than RRP-8220 (but comparable Nb:Sn ratio), so the A15 area formed after reaction and consequently non-copper J_c are lower than for RRP-8220. The smaller sub-elements also reduce the distance required for Sn and Ti to diffuse.

Table II summarizes the results for this billet. Here too we find that a temperature increase of 15 °C produces equivalent properties in half the time. T_c values are in the range expected for 2.4% Ti alloying [13], although it has been argued that the annulus average over-estimates the actual Ti amount incorporated into the A15 phase [9]. Surprisingly, T_c values are rather insensitive to reaction temperature. Since we observe dramatic effects of alloying in the H_K values, this implies that Ti diffuses rapidly throughout the A15 region even at temperatures for which tin diffusion is sluggish.

Also, H_K is comparatively higher for RRP-8079 than for RRP-8220 for the 650/48 and 665/48 (665/50) reactions used to optimize J_c, e.g. 25.1 and 26.8 T for RRP-8079 vs. 23.1 and

TABLE II. SUMMARY OF REACTION PARAMETERS AND MEASUREMENTS FOR TI-ALLOYED AND TI+TA-ALLOYED STRANDS

Temp	Time	J_c(12T)	RRR	H_K	T_c	ΔT_c	$F_{p,max}$
°C	h	A/mm^2		T	K	K	GN/m^3
			RRP-8079				
635	36	2325	344	23.4			49.7
635	48	2457	356	23.9	16.3	1.08	56.6
650	48	2587	214	25.1	16.43	1.00	55.6
650	96	2664	30	26.0	16.49	1.27	49.1
650	144	2806	12	26.7	16.58	1.04	50.1
665	48	2709	80	26.4	16.50	0.85	49.0
695	48	2675	20	27.5	16.56	1.05	51.3
			RRP-9415				
665	48	3009	358	26.3	16.83	1.10	54.4
			RRP-9362				
665	48	2818	169	26.8	16.52	1.28	49.9

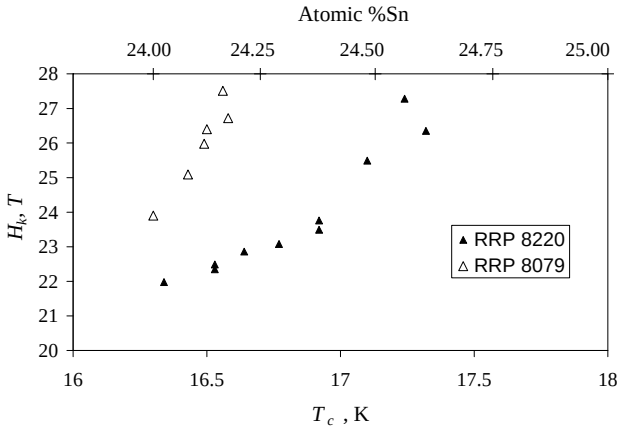

Fig. 5. H_K versus T_c for 8220 and 8079 samples. The upper axis shows the Sn composition inferred from the T_c using Devantay's relation. (1).

23.8 T for RRP-8220 respectively. Yet, at the highest reaction temperatures both have similar H_K of ~ 27.5 T at 4.2 K. Fig. 5 shows a comparison of how H_K and T_c for the two different strand designs. These data suggest Ti alloying may be better for optimizing properties at high field with 48-hour reactions than Ta alloying.

We compared 665/48 reactions for RRP-9415 and RRP-9362 to those for RRP-8220. The T_c transitions, shown in Fig. 6, show that progressively stronger alloying results in lower T_c. However, these changes are minor compared to the >3 T gains in H_K (Table II) while still maintaining ~3000 A·mm^{-2} performance at 12 T, 4.2 K. Clearly, the addition of Ti has a strong benefit for ~15 T and higher field magnets. In fact, the pinning-force data extrapolate to J_c values for the Ti-alloyed wires that are well above the performance of RRP-8220 for H > 15 T. Ti alloying is clearly essential for very high-field magnet strands.

None of the Ti-alloyed billets attained $F_{p,\,max}$ levels as high as for the Ta-alloyed RRP-8220. Given that H_K is higher, this points to either a reduction of the grain-boundary density or a reduction of the specific grain-boundary pinning force.

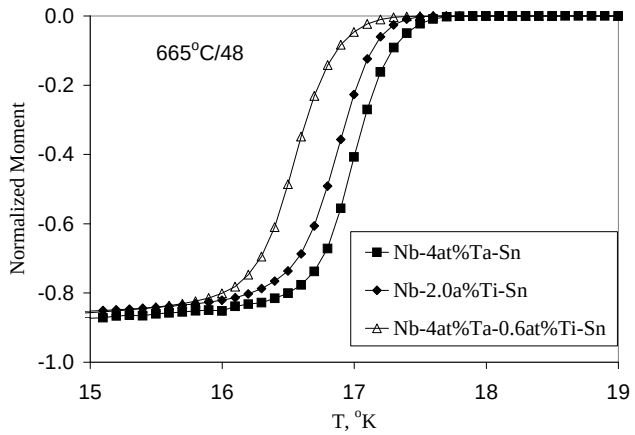

Fig. 6. Plot of normalized moment for wires with different compositions using the 665/48 reaction.

IV. Conclusion

This investigation shows that the maximum J_c of the RRP conductor at ~0.5H_K can be attained by multiple time-temperature pathways between ~620 to 665 °C. The average Sn composition in the A15 is close to 25%, with low Sn gradients. Maximum pinning is a compromise between the density of pinning sites and the superconducting properties like T_c and H_K. For 15 T and beyond, the Ta-ternary requires higher reaction temperatures to increase H_K and T_c, but these gains cannot offset losses due to grain growth. On the other hand, Ti-alloying provides higher H_K at the reaction temperatures where $F_{p,max}$ remain high. Therefore, Ti alloying needs further development to optimize the alloy composition and wire processing.

Acknowledgment

A.K.G. and L.D.C. thank D. Dietderich for providing the wires from the CDP inventory, and J. Parrell, and S. Hong of OST for discussions about the different billets.

References

[1] S. A. Gourlay *et al*., "Magnet R&D for the US LHC Accelerator Research Program (LARP)", *IEEE Trans. Appl. Supercond*, ., vol. 13, pp. 324-327,2006

[2] J. A. Parrell, Y. Zhang, R. W. Hentges, M. B. Field and S. Hong, "Nb_3Sn strand development at Oxford Superconducting Technology", *IEEE Trans. Appl. Supercond*., vol. 13, pp. 3470-3473, 2003.

[3] M. T. Naus, P. J. Lee, and D. C. Larbalestier, "The Influence of the Starting Cu-Sn Phase on the Superconducting Properties of Subsequently Reacted Internal- Sn Nb3 Sn Conductors", *IEEE Trans. Appl. Supercond*, vol. 11, pp. 3569-3572, ,2000.

[4] C, D. Hawes, P. J. Lee, and D. C. Larbalestier, "Measurement of the Critical Temperature Transition and Composition Gradient in Powder-In-Tube NbsSn Composite Wire", *IEEE Trans. Appl. Supercond*, ., vol. 10, pp. 988-991,2000

[5] L. D. Cooley, C. M. Fischer, P. J. Lee, and D. C. Larbalestier, "Simulations of the effects of tin composition gradients on the superconducting properties of Nb3Sn conductors", *J. of Appl. Phys*., fol. 96, pp. 2122-2130, 2004.

[6] C. M. Fischer, P. J. Lee and D. C. Larbalestier, "Irreversibility field and critical current density as a function of heat reatment time and temperature for a pure Niobium powder-in-tube conductor", *Adv. in Cryo. Eng*. Vol. 48, pp. 1008-1014, 2002

[7] P. J. Lee and D. C. Larbalestier "Microstructure, Microchemistry and the Development of Very High Nb3Sn Layer Critical Current Density", *IEEE Trans. Appl. Supercond*, ., vol. 15, pp. 3474-3477 ,2005

[8] R. M. Scanlan, "Conductor development for High Energy Physics-Plans and status of the U. S. Program", *IEEE Trans. Appl. Supercond*, vol. 11, p. 2150, 2001.

[9] J. A. Parrell, M. B. Field, , and Y. Zhang S. Hong, "Advances in Nb3Sn Strand for Fusion and Particle Accelerator Applications", *IEEE Trans. Appl. Supercond*, vol. 16, p. 1200-1204, 2005.

[10] R. Soika, L. D. Cooley, A. K. Ghosh, and A. Werner, "Fixture for short sample testing of modern high energy physics Nb_3Sn strands", *Adv. Cryo. Eng. (Materials)*, vol. 50A, pp. 67 – 74, 2004.

[11] H. Devantay, J. L. Jorda, M. Decroux, J. Muller, "The physical and structural properties of superconducting A15-type Nb- Sn alloys," J. Mat. Sci., v0l. 16, pp. 2145-2153, 1981.

[12] A. K. Ghosh, L. D. Cooley, J. A. Parrell, M. B. Field, Y. Zhang, and S. Hong, "Effects of Reaction Temperature and Alloying on Performance of Restack-rod-process Nb3Sn", *", IEEE Trans. Appl. Supercond*, vol. 17, p. 2623, 2007.

[13] M. Suenaga, "Optimization of Nb3Sn", *IEEE Trans, on Magnetics*, Vol. 21, pp.1122-1128, 1985.